Comparative analysis of magnetic resonance in the polaron pair recombination and the triplet exciton-polaron quenching models

V. V. Mkhitaryan,[1,*] D. Danilović,[1] C. Hippola,[1] M. E. Raikh,[2] and J. Shinar[1]
[1]*Ames Laboratory, Iowa State University, Ames, Iowa 50011, USA*
[2]*Department of Physics and Astronomy, University of Utah, Salt Lake City, Utah 84112, USA*

(Received 17 August 2017; revised manuscript received 14 November 2017; published 3 January 2018)

We present a comparative theoretical study of magnetic resonance within the polaron pair recombination (PPR) and the triplet exciton-polaron quenching (TPQ) models. Both models have been invoked to interpret the photoluminescence detected magnetic resonance (PLDMR) results in π-conjugated materials and devices. We show that resonance line shapes calculated within the two models differ dramatically in several regards. First, in the PPR model, the line shape exhibits unusual behavior upon increasing the microwave power: it evolves from fully positive at weak power to fully negative at strong power. In contrast, in the TPQ model, the PLDMR is completely positive, showing a monotonic saturation. Second, the two models predict different dependencies of the resonance signal on the photoexcitation power, P_L. At low P_L, the resonance amplitude $\Delta I/I$ is $\propto P_L$ within the PPR model, while it is $\propto P_L^2$ crossing over to P_L^3 within the TPQ model. On the physical level, the differences stem from different underlying spin dynamics. Most prominently, a negative resonance within the PPR model has its origin in the microwave-induced spin-Dicke effect, leading to the resonant quenching of photoluminescence. The spin-Dicke effect results from the spin-selective recombination, leading to a highly correlated precession of the on-resonance pair partners under the strong microwave power. This effect is not relevant for TPQ mechanism, where the strong zero-field splitting renders the majority of triplets off resonance. On the technical level, the analytical evaluation of the line shapes for the two models is enabled by the fact that these shapes can be expressed via the eigenvalues of a complex Hamiltonian. This bypasses the necessity of solving the much larger complex linear system of the stochastic Liouville equations. Our findings pave the way towards a reliable discrimination between the two mechanisms via cw PLDMR.

DOI: 10.1103/PhysRevB.97.035402

I. INTRODUCTION

Over the years, optically detected magnetic resonance (ODMR) has proven to be a powerful tool for the study of spin-dependent recombination and dissociation processes, both in inorganic [1–3] and in organic [4] semiconductors. High sensitivity, exceeding the sensitivity of conventional electron spin resonance by about 6 orders of magnitude, renders ODMR the tool of choice when it comes to π-conjugated polymers [4], where the density of spin carriers is small. Photoluminescence detected magnetic resonance (PLDMR), being a subset of ODMR, has an advantage as it provides the most straightforward probe of the radiative singlet exciton population and quantum yield of the material [4–7]. Besides, this method is suitable for probing the bulk of a photoluminescent material without the necessity of device fabrication.

Two different models have been employed to explain PLDMR results in π-conjugated materials. The double-modulation PLDMR experiment [6] advocated the quenching model based on the spin-dependent reaction between triplet excitons and polarons. On the other hand, the experimental study of the frequency dependence of the in-phase component of PLDMR [7] employed the polaron pair recombination model. Subsequent publications invoked both the quenching model [8,9] and the recombination model [10] for the interpretation of results obtained for the same material, polymer MEH-PPV.

In order to distinguish between the two models, pulsed PLDMR experiments were conducted [11] in which Rabi beats of PLDMR in MEH-PPV and its deuterated variant were explored. The results appear to reveal the fingerprints of both the recombination and the quenching mechanisms. Hence, for conclusive discrimination, additional continuous-wave PLDMR measurements revealing the nature of the underlying spin-dependent processes are desirable. Equally, theoretical predictions of the differences in the PLDMR within the two models are highly desirable. That is the goal of the present paper. To achieve this goal, we employ the stochastic Liouville equations for the density matrix to calculate analytically the resonance line shapes and saturation within the recombination and quenching models. We show how the difference in the underlying spin dynamics translates into very different dependencies of the PLDMR on the optical excitation intensity. Also, within the recombination model, the line shape is predicted to be very peculiar, with a peak precisely at the resonant frequency evolving into a minimum at higher microwave power.

Our results on the dynamics of the spin pairs within the polaron recombination model agree with the predictions based on the analysis of eigenmodes for the calculation of transport [12,13] and with a direct analytical solution of the Liouville equations [14,15]. At the same time, Refs. [12,13] do not employ the density matrix formalism at all. Instead, the

*Corresponding author: vmkhitar@ameslab.gov

spin-dependent recombination is incorporated into the equation of motion for the amplitude of the singlet. References [14,15] study the dynamics of electron- and hole-polaron spins with different g factors and do not consider the random local hyperfine fields at all. This makes the polaron pair spin dynamics very different from that considered in the present work, where the electron and hole g factors are practically indistinguishable, and the singlet-triplet interconversion is governed by the local hyperfine fields.

We consider the regime relevant to fluorescent π-conjugated polymers. According to experiments, this regime is characterized by very close electron- and hole-polaron g factors [10,16], relatively strong hyperfine interaction [11,16,17], relatively slow recombination from the singlet polaron pair state [7,17], relatively slow annihilation of triplet excitons from doublet triplet-polaron state [6,8], relatively long spin coherence times [16,17], weak exchange [18], and weak dipolar interaction between polaron pair or exciton-polaron spins [6,9,18], etc.

Our analytical results can be directly generalized to include a broader class of ODMR techniques, as well as other detection methods, e.g., electrical, reaction yield, and capacitance measurements. In this connection, notice the similarity between our results for the polaron pair recombination model and those observed in recent transport [19] and dielectric polarizability [20] studies.

The established substantial differences between the predictions of the polaron pair recombination and triplet exciton-polaron quenching models can enable the differentiation of the two mechanisms in interpretation of continuous-wave PLDMR results.

II. THE POLARON PAIR RECOMBINATION MODEL

A. Qualitative picture

The PPR model is illustrated in Fig. 1. The processes involved are the generation of weakly coupled polaron pairs (PP)

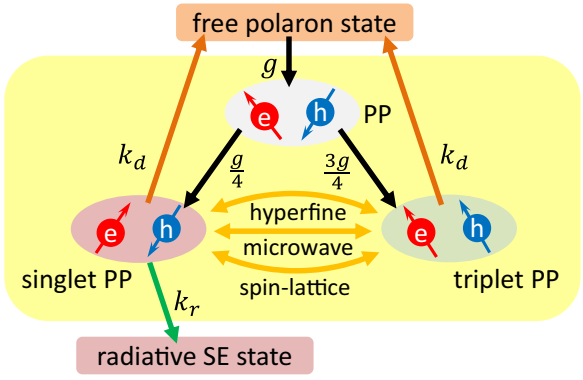

FIG. 1. Schematics of the processes underlying the PPR model. The black arrows indicate the PP generation; out of g PPs per second, $\frac{g}{4}$ are singlets and $\frac{3g}{4}$ are triplets. The brown and green arrows respectively indicate the dissociation and recombination, Eq. (10). The orange arrows represent the singlet-triplet beating, induced by the hyperfine coupling and resonance microwave, Eq. (9), and the spin-lattice relaxation, Eq. (11). The yellow background outlines the components of the stochastic Liouville equation (8).

at rate g, their dissociation with at rate k_d, and recombination from the singlet pair state at rate k_r [21]. The latter process constitutes the reaction

$$\mathrm{P}_e + \mathrm{P}_h \rightarrow \mathrm{S} \tag{1}$$

between the electron and hole polarons, P_e and P_h, respectively, yielding a singlet exciton, S. Thus, the spin-selective recombination is incorporated as the restriction that Eq. (1) can occur only for singlet PPs, i.e., for triplet PPs it is forbidden.

In an applied static magnetic field, $\mathbf{B}_0 = B_0\hat{\mathbf{z}}$, the electron- and hole-polaron spin-up ($|\uparrow\rangle_e$ and $|\uparrow\rangle_h$) and spin-down ($|\downarrow\rangle_e$ and $|\downarrow\rangle_h$) states occupy the Zeeman levels, $\frac{1}{2}\hbar\gamma B_0$ and $-\frac{1}{2}\hbar\gamma B_0$, respectively, where γ is the polaron gyromagnetic ratio (we assume equal gyromagnetic ratios for the electron and hole polarons). The triplet-singlet PP spin states,

$$\begin{aligned} |T_+\rangle &= |\uparrow\rangle_e|\uparrow\rangle_h, \quad |T_-\rangle = |\downarrow\rangle_e|\downarrow\rangle_h, \\ |T_0\rangle &= \frac{1}{\sqrt{2}}(|\uparrow\rangle_e|\downarrow\rangle_h + |\downarrow\rangle_e|\uparrow\rangle_h), \\ |S\rangle &= \frac{1}{\sqrt{2}}(|\uparrow\rangle_e|\downarrow\rangle_h - |\downarrow\rangle_e|\uparrow\rangle_h), \end{aligned} \tag{2}$$

form a convenient basis for the discussion of magnetic-field effects. The resonant microwaves couple the Zeeman levels of individual spins and, correspondingly, the triplet PP levels. On the other hand, random hyperfine fields created by the nuclei (almost entirely hydrogen protons) at electron- and hole-polaron sites induce interconversion between the singlet and triplet PP levels. Characteristic magnitudes of these hyperfine fields $b_{\mathrm{hf},e}$ and $b_{\mathrm{hf},h}$ are different in general and define two distinct hyperfine frequencies, $\omega_{\mathrm{hf},\mu} = \gamma b_{\mathrm{hf},\mu}$, $\mu = e, h$.

If the pair spins are uncorrelated, the populations of individual Zeeman levels in the microwave drive field $\mathbf{B}_1(t) = 2B_1\cos(\omega t)\hat{\mathbf{x}}$ oscillate with Rabi frequencies

$$\Omega_\mu = \sqrt{\omega_\mu^2 + \omega_1^2}, \quad \mu = e, h, \tag{3}$$

where $\omega_1 = \gamma B_1$ is the microwave drive amplitude, and

$$\omega_\mu = \gamma b_{z,\mu} + \delta, \quad \delta = \gamma B_0 - \omega, \tag{4}$$

are the polaron Larmor frequencies in the rotating frame and the detuning frequency, respectively. The z components of the random hyperfine fields $b_{z,\mu}$ follow a Gaussian distribution, entailing a Gaussian distribution of Larmor frequencies:

$$\mathcal{N}(\omega_\mu) = \frac{1}{\sqrt{2\pi}\,\omega_{\mathrm{hf},\mu}} e^{-(\omega_\mu-\delta)^2/2\omega_{\mathrm{hf},\mu}^2}, \quad \mu = e,h. \tag{5}$$

The most important physics of the PPR model is that the spin-selective recombination correlates the dynamics of each of the spins in the pair. Indeed, if the recombination rate was the same for all four spin-pair states, then the Rabi beatings of the level populations would not affect the luminescence, and therefor no PLDMR would be detectable.

The essence of PLDMR technique is that the intensity of recombination shown in Fig. 1 exhibits a resonance as a function of δ, which becomes progressively pronounced as the microwave field amplitude ω_1 exceeds $\omega_{\mathrm{hf},\mu}$. The PLDMR amplitude is directly related to the singlet exciton density n_{S}. Therefore, the evaluation of resonance line shapes reduces to finding n_{S} versus δ, ω_1, and $\omega_{\mathrm{hf},\mu}$. One can naturally distinguish

two regimes: weak drive, $\omega_1 \ll \omega_{\mathrm{hf},\mu}$, and strong drive, $\omega_1 \gg \omega_{\mathrm{hf},\mu}$. It might seem that at weak drive Rabi oscillations do not occur. However, as the hyperfine fields are random, some spins will be at resonance. Their fraction can be estimated as [16,21,22] $\sim\omega_1/\omega_{\mathrm{hf},\mu}$. Our main result for weak drive is that these pairs dominate the resonance line shape, leading to the linear dependence of the resonance amplitude on ω_1. This conclusion contrasts with the results obtained from simple rate equations [7] and from other studies of PP spin dynamics and recombination that exclude averaging over local hyperfine fields [14,23].

In the strong drive regime, the physics underlying the resonance line shape is different. In this regime, not only are the four conventional spin-pair states not eigenstates, but actually $(|T_{+1}\rangle - |T_{-1}\rangle)/\sqrt{2}$ is close to an eigenstate, and it is decoupled from $|S\rangle$. This means it is a long-lived state. We will see that this decoupling is a consequence of the spin-Dicke effect [12,13]. It manifests itself as a minimum in the resonance line shape at zero detuning, which gradually takes over as the microwave drive increases, turning the resonance to fully negative.

More formally, under steady-state conditions, the photoluminescence intensity $\mathcal{I}$ is proportional to the steady-state singlet density, $\tilde{n}_{\mathrm{S}}$. The latter is found from the rate equation

$$\partial_t n_{\mathrm{S}} = G_S - R_S n_{\mathrm{S}} + \alpha(\delta,\omega_1), \tag{6}$$

where G_S is the photoexcitation rate of singlet excitons, R_S is their decay rate, and $\alpha(\delta,\omega_1)$ is the rate of singlet exciton generation due to the PPR, Eq. (1), rendering the PLDMR within the PPR model. The normalized PLDMR is then given by

$$\frac{\Delta\mathcal{I}(\delta,\omega_1)}{\mathcal{I}(0)} = \frac{\tilde{n}_{\mathrm{S}}(\delta,\omega_1) - \tilde{n}_{\mathrm{S}}(0)}{\tilde{n}_{\mathrm{S}}(0)} = \frac{\alpha(\delta,\omega_1) - \alpha(0)}{G_S}, \tag{7}$$

where the relation $G_S \gg \alpha$, common for many systems [4], is used in the last equality, and zero arguments correspond to $\omega_1 = 0$, implying the absence of microwave drive; $\alpha(\delta,\omega_1)$ is governed by the spin dynamics of polaron pairs, to which we turn next.

B. Spin dynamics of weakly coupled electron-hole pair ensemble

The spin dynamics of a PP ensemble is analyzed by solving the stochastic Liouville equation for the spin density matrix ρ,

$$\frac{d\rho}{dt} = i[\rho,H] + \frac{g}{4}\mathbb{1} + \mathcal{R}_{\mathrm{dr}}\{\rho\} + \mathcal{R}_{\mathrm{sl}}\{\rho\}, \tag{8}$$

where the first term describes the spin dynamics due to the magnetic interactions governed by the spin Hamiltonian H, g is the PP generation rate, $\mathbb{1}$ is the identity operator, $\mathcal{R}_{\mathrm{dr}}$ represents the pair dissociation and recombination, and $\mathcal{R}_{\mathrm{sl}}$ the spin-lattice relaxation processes. [For the discussion of the relation between Eq. (8) and a more general Lindblad equation see Appendix A.]

For simplicity, we neglect the spin exchange and dipolar interactions. (Generalization for the nonzero spin exchange and dipolar interactions will be discussed later.) In the rotating frame, the spin Hamiltonian is given by

$$H = \omega_e S_e^z + \omega_h S_h^z + \omega_1\left(S_e^x + S_h^x\right), \tag{9}$$

where ω_e and ω_h are local electron and hole detunings, see Eq. (4). They are different due to the different on-site hyperfine fields. $\mathbf{S}_{e,h}$ stands for the electron- and hole-polaron spin operators (we set $\hbar = 1$).

Conventionally, the spin-dependent recombination processes are described within the singlet-triplet basis of PP. We assume that the pair dissociation occurs at the equal rate k_d from all spin states. In terms of the matrix elements we have

$$\mathcal{R}_{\mathrm{dr}}\{\rho\}_{\alpha\beta} = -k_d\rho_{\alpha\beta} - \frac{k_r}{2}(\delta_{\alpha S} + \delta_{S\beta})\rho_{\alpha\beta}, \tag{10}$$

where $\alpha,\beta = +1,-1,0$, and S enumerate the singlet and triplet spin states $|T_{+1}\rangle$, $|T_{-1}\rangle$, $|T_0\rangle$, and $|S\rangle$, respectively.

For the spin-lattice relaxation we take the form [14]

$$\mathcal{R}_{\mathrm{sl}}\{\rho\}_{\alpha\beta} = -(1/T_{\mathrm{sl}})[\rho_{\alpha\beta} - \delta_{\alpha\beta}\mathrm{tr}(\rho/4)]. \tag{11}$$

This relaxation tends to equalize the state populations, with the rate $1/T_{\mathrm{sl}}$.

As an important step, we introduce the complex Hamiltonian,

$$\mathcal{H} = H - i(w_d/2)\mathbb{1} - i(k_r/2)\Pi_S, \tag{12}$$

where $w_d = k_d + 1/T_{\mathrm{sl}}$ and $\Pi_S = |S\rangle\langle S|$ is the projection operator onto the singlet state. In terms of the complex Hamiltonian, Eq. (8) for the density matrix takes the form

$$\frac{d\rho}{dt} = i(\rho\mathcal{H}^* - \mathcal{H}\rho) + \frac{1}{4}\left(g + T_{\mathrm{sl}}^{-1}\mathrm{tr}\rho\right)\mathbb{1}. \tag{13}$$

The observable quantities are described by the steady-state density matrix $\tilde{\rho}$, satisfying

$$i(\tilde{\rho}\mathcal{H}^* - \mathcal{H}\tilde{\rho}) + \tfrac{1}{4}\left(g + T_{\mathrm{sl}}^{-1}\mathrm{tr}\tilde{\rho}\right)\mathbb{1} = 0. \tag{14}$$

We write the formal solution of Eq. (14) as

$$\tilde{\rho} = \frac{1}{4}\left(g + T_{\mathrm{sl}}^{-1}\mathrm{tr}\tilde{\rho}\right)U, \quad U = \int_0^\infty dt\, e^{-i\mathcal{H}t}e^{i\mathcal{H}^*t}. \tag{15}$$

Thus, the matrix structure of $\tilde{\rho}$ is posed by U. Another useful relation is found by taking the trace of the right-hand side of Eq. (14):

$$g - k_d\mathrm{tr}\tilde{\rho} - k_r\tilde{\rho}_{SS} = 0, \tag{16}$$

where $\tilde{\rho}_{SS} = \langle S|\tilde{\rho}|S\rangle$ is the singlet polaron pair population. Equation (16) is the balance equation between the generation of PPs and their destruction, taking place from the triplet and singlet states with the rates k_d and $k_d + k_r$, respectively. From Eqs. (15) and (16) we find

$$k_r\tilde{\rho}_{SS} = gL(\delta,\omega_1), \quad L = \frac{1 - (w_d/4)\mathrm{tr}U(\delta,\omega_1)}{1 - (1/4T_{\mathrm{sl}})\mathrm{tr}U(\delta,\omega_1)}. \tag{17}$$

As will be seen shortly, Eqs. (15) and (17) are sufficient for the calculation of $\alpha(\delta,\omega_1)$, which is the resonance line shape. Most importantly, we will need only the eigenvalues of 4×4 complex Hamiltonian $\mathcal{H}$. This bypasses the necessity of solving effectively a 10×10 complex system of linear equations (14).

The calculation of resonance line shape, $\alpha(\delta,\omega_1)$, involves also the averaging over the Gaussian distribution of hyperfine

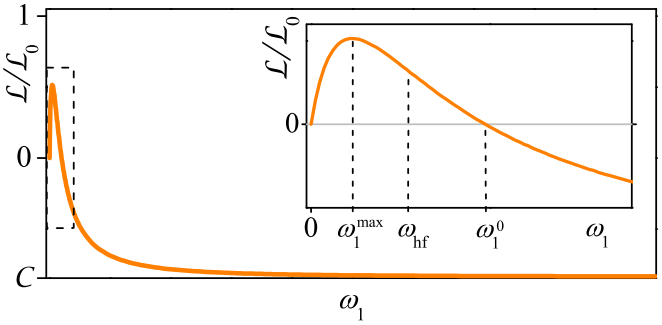

FIG. 2. Sketch of the function $\mathcal{L}(0,\omega_1)$ defining the PLDMR amplitude at zero detuning [see Eq. (19)] in units of $\mathcal{L}_0$, Eq. (38). The constant $\mathcal{C}$, Eq. (41), is the saturation value of $\mathcal{L}(0,\omega_1)/\mathcal{L}_0$. The inset zooms into the region indicated in the main panel with a dashed rectangle.

Larmor frequencies, Eq. (5):

$$\alpha(\delta,\omega_1) = k_r\langle\tilde{\rho}_{SS}\rangle_{\rm hf} = g\langle L(\delta,\omega_1)\rangle_{\rm hf}. \tag{18}$$

Furthermore, for the PP generation rate one has $g \propto \tilde{n}_{\rm P}^2$, where $\tilde{n}_{\rm P}$ is the steady-state density of polarons. Thus, from Eqs. (7) and (18) we write

$$\frac{\Delta\mathcal{I}}{\mathcal{I}} = \frac{\lambda_P\tilde{n}_{\rm P}^2}{G_S}\mathcal{L}(\delta,\omega_1), \quad \mathcal{L} = \langle L(\delta,\omega_1) - L(0)\rangle_{\rm hf}, \tag{19}$$

where the constant λ_P is determined by the PP formation cross section, proportional to the polaron mobility.

From now on we focus on the regime of weak recombination, $k_r \ll \omega_{\rm hf}$. Still, before going into the details of analytical calculation, in Fig. 2 we outline the typical result obtained by solving Eq. (14) and performing the averaging in Eq. (18) numerically. Note that the curve in Fig. 2 is a sketch for model parameters in the regime of weak recombination. [For an actual plot with particular model parameters we refer to Figs. 3 and 5(a).] The plot in Fig. 2 shows a steep increase at weak $\omega_1 \ll \omega_{\rm hf}$, a maximum followed by a moderate decrease at $\omega_1 \gtrsim \omega_{\rm hf}$, and a very slow decrease to negative values with saturation at the strongest drives. This picture appears to be quite general for a wide range of model parameters. In addition, in the limits of weak and strong drive the curve can be described analytically. This is accomplished in the next section.

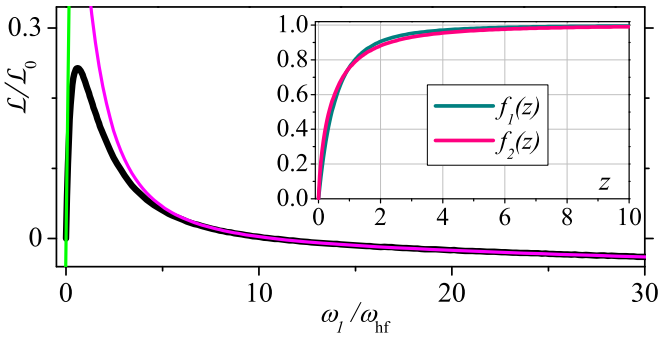

FIG. 3. The PLDMR amplitude at zero detuning $\mathcal{L}(\omega_1)$, found by numerically solving the Liouville Eq. (14), is plotted in black, together with the weak-driving asymptote, Eq. (39) [green], and the strong-driving asymptote, Eq. (44) [magenta]. The parameters are set to $w_d \equiv k_d + 1/T_{\rm sl} = 30$ kHz, $k_r = 230$ kHz, and $\omega_{\rm hf}/2\pi = 16.8$ MHz, corresponding to the hyperfine field of 6 Gauss. Inset: Plots of the universal functions, Eqs. (42) and (43).

C. Perturbation with respect to small k_r

In the limit of slow recombination, $k_r \ll \omega_{\rm hf}$, the perturbative approach applies. The unperturbed eigenstates of $\mathcal{H}$ are the eigenvectors of the Hamiltonian (9):

$$H|\varphi_\alpha\rangle = \epsilon_\alpha|\varphi_\alpha\rangle, \quad \alpha = 1,\ldots,4. \tag{20}$$

In the absence of recombination the pair partners are independent, so that the eigenvalues are given by

$$\epsilon_1 = -\epsilon_4 = \tfrac{1}{2}(\Omega_e + \Omega_h), \quad \epsilon_2 = -\epsilon_3 = \tfrac{1}{2}(\Omega_e - \Omega_h), \tag{21}$$

where $\Omega_{e,h}$ are defined by Eq. (3).

In the presence of recombination, the eigenvectors are perturbed by the operator $V = -i(k_r/2)\Pi_S$, which is responsible for this process. The matrix form of this operator, $V_{\alpha\beta} = \langle\varphi_\alpha|V|\varphi_\beta\rangle$, is found in Appendix B. It is conveniently parameterized by the angles,

$$\tan 2\phi_\mu = \frac{\omega_1}{\omega_\mu}, \quad \mu = e,h. \tag{22}$$

The explicit form of the matrix reads

$$V = -i\frac{k_r}{4}\frac{1}{1+\xi^2}\begin{pmatrix} \xi^2 & \xi & -\xi & \xi^2 \\ \xi & 1 & -1 & \xi \\ -\xi & -1 & 1 & -\xi \\ \xi^2 & \xi & -\xi & \xi^2 \end{pmatrix}, \tag{23}$$

where

$$\xi = \tan(\phi_{\rm eh}), \quad \phi_{\rm eh} = \phi_e - \phi_h. \tag{24}$$

The leading recombination-induced corrections to the eigenvalues Eq. (21) are given by the diagonal elements,

$$\epsilon_{1,4}^{(1)} = -i\frac{k_r}{4}\sin^2\phi_{\rm eh}, \quad \epsilon_{2,3}^{(1)} = -i\frac{k_r}{4}\cos^2\phi_{\rm eh}. \tag{25}$$

According to the standard perturbation theory [24], the eigenstates of $\mathcal{H}$ are close to $|\varphi_\alpha\rangle$, when $|\epsilon_\alpha - \epsilon_\beta| \gg k_r$ for $\alpha \neq \beta$. Here we make a crucial observation that for certain pairs for which Ω_e and Ω_h are anomalously close, this condition is violated. Such a "softening" of modes manifests the degeneracy in the perturbation theory. As a result, the eigenstates of $\mathcal{H}$ strongly deviate from $|\varphi_2\rangle$ and $|\varphi_3\rangle$, and are determined by the small V.

The condition of softening is progressively satisfied as the drive increases. This is because $|\Omega_e - \Omega_h| \approx |\omega_e^2 - \omega_h^2|/2\omega_1$ decreases with drive. As a result, $|\varphi_2\rangle$ and $|\varphi_3\rangle$ are close to

$$\tfrac{1}{2}(|T_{+1}\rangle - |T_{-1}\rangle \pm \sqrt{2}|S\rangle), \tag{26}$$

whereas the corresponding eigenstates of $\mathcal{H}$ are close to

$$\frac{1}{\sqrt{2}}(|T_{+1}\rangle - |T_{-1}\rangle) \quad \text{and} \quad |S\rangle. \tag{27}$$

This in turn suppresses the overall recombination. It is important to emphasize that the strong modification of eigenstates and the entailing lifetime anomaly is the consequence of the backaction of recombination on the quantum dynamics of PP spins. As pointed out in Refs. [12,13], there is a

close analogy between the long-living states and the subradiant modes in the Dicke effect [25]. In previous studies of spin-dependent recombination this backaction is neglected (see, e.g., Ref. [26]).

The region of strong drive, where $|\Omega_e - \Omega_h| \lesssim k_r$, is difficult to access because of the degeneracy. The difficulty is circumvented in the following way. Neglecting all the off-diagonal elements of Eq. (23), except for V_{23} and V_{32}, induces an error in eigenstates and eigenvalues only of the order of k_r/Ω_μ and k_r^2/Ω_μ, respectively, whereas the result for $\mathrm{tr}\, U$ remains correct to the leading order. (This is analogous to the secular approximation widely used in the theory of magnetic resonance [27].) Therefore we proceed by replacing $V = -i(k_r/2)\Pi_S$ in Eq. (12) with

$$\tilde{V} = -i\frac{k_r}{4}\frac{1}{1+\xi^2}\begin{pmatrix}\xi^2 & 0 & 0 & 0\\ 0 & 1 & -1 & 0\\ 0 & -1 & 1 & 0\\ 0 & 0 & 0 & \xi^2\end{pmatrix}. \tag{28}$$

This replacement retains all the eigenvalues and eigenvectors of $\mathcal{H}$ to the leading order and allows the direct evaluation of the operator U from Eq. (15). We find

$$\begin{aligned}&\mathrm{tr}\, U(\delta,\omega_1)\\ &= \frac{4(4w_d + k_r)}{4w_d^2 + 2w_d k_r + \left(k_r^2/4\right)\sin^2(2\phi_{\mathrm{eh}})}\\ &\quad + \frac{k_r^2\cos^4(\phi_{\mathrm{eh}})}{[k_r\cos^2(\phi_{\mathrm{eh}}) + 2w_d]\left[4\epsilon_2^2 + w_d(k_r\cos^2(\phi_{\mathrm{eh}}) + w_d)\right]}.\end{aligned} \tag{29}$$

[As shown in Appendix B, the replacement of V by $\tilde{V}$ amounts to $\sim(k_r/\Omega_\mu)^2$ order terms, so that Eq. (29) is highly accurate.] Notably, the δ and ω_1 dependence of $\mathrm{tr}\, U$ enters in Eq. (29) via the angles ϕ_{eh} and the energy ϵ_2. The analytical expression Eq. (29) is the main result of this section. We emphasize again that it is derived without solving the 10×10 equation (14).

The microscopic origin of the two terms in Eq. (29) is easy to trace back. The first term comes from the diagonals of V and describes the interplay of spin dynamics and recombination far from the degeneracy. This term is dominant at weak and moderate drive, $\omega_1 \lesssim \omega_{\mathrm{hf}}$. The second term originates from the off-diagonal elements, V_{23} and V_{32}, and becomes important with the onset of degeneracy. It quantifies the microwave-induced Dicke effect, prevailing at strong drive, $\omega_1 > \omega_{\mathrm{hf}}$.

The first term in Eq. (29) is monotonically decreasing function of $\sin^2 2\phi_{\mathrm{eh}}$. At the same time, the second term in Eq. (29) is monotonically increasing function of $\cos^2\phi_{\mathrm{eh}}$. This observation yields the estimate

$$\frac{16}{4w_d + k_r} \leqslant \mathrm{tr}\, U \leqslant \frac{4w_d + 3k_r}{w_d(w_d + k_r)}, \tag{30}$$

for the upper and lower bounds of $\mathrm{tr}\, U$. For $k_r \ll w_d$, the left and right sides of Eq. (30) are both close to $4/w_d$, while they are quite different in the opposite limit, $k_r \gg w_d$. This means that, in the first case, magnetic resonance can induce only weak relative variations of $\mathrm{tr}\, U$, and therefore of α, whereas a considerable relative change in α is possible in the latter limit.

D. Averaging over the random hyperfine fields for slow spin-lattice relaxation

We defer the discussion of finite spin relaxation to the end of this section and proceed with the case of long coherence time, $T_{\mathrm{sl}} \gg k_d^{-1}, k_r^{-1}$. From Eq. (30) it follows that in this case $(1/4T_{\mathrm{sl}})\,\mathrm{tr}U \ll 1$, so that the denominator of Eq. (17) can be treated perturbatively, yielding

$$L = 1 - (k_d/4)\mathrm{tr}U. \tag{31}$$

Thus, finding the hyperfine average, $\langle L\rangle_{\mathrm{hf}}$, reduces to averaging of Eq. (29) over the Gaussian distribution of Larmor frequencies:

$$\langle \mathrm{tr}U\rangle_{\mathrm{hf}} = \int d\omega_e d\omega_h \mathcal{N}(\omega_e)\mathcal{N}(\omega_h)\,\mathrm{tr}U(\delta,\omega_1). \tag{32}$$

(For simplicity we assume that the mean square deviations of the Gaussian distributions are the same, $\omega_{\mathrm{hf},e} = \omega_{\mathrm{hf},h} = \omega_{\mathrm{hf}}$, unless it is stated otherwise.)

1. Zero detuning

For zero detuning, $\delta = 0$, the random variables $x = (\omega_e + \omega_h)/2\omega_1$ and $y = (\omega_e - \omega_h)/2\omega_1$ have the same Gaussian distribution,

$$\mathcal{P}(x) = \frac{1}{\sqrt{\pi}\beta_0}\exp\left(-x^2/\beta_0^2\right), \quad \beta_0 = \frac{\omega_{\mathrm{hf}}}{\omega_1}. \tag{33}$$

Relevant quantities entering in Eq. (29) are given by

$$\sin^2(2\phi_{\mathrm{eh}}) = \frac{4y^2}{(1+x^2-y^2)^2 + 4y^2} \tag{34}$$

and

$$\varepsilon_2 = \frac{\omega_1}{2}\left(\sqrt{1+(x+y)^2} - \sqrt{1+(x-y)^2}\right). \tag{35}$$

Below, the averaging is performed analytically, in the limits of weak and strong drive.

2. Weak resonant drive, $\omega_1 \ll \omega_{hf}$

In the limit of weak drive the second term of Eq. (29) is negligible, because the PP realizations with $4\varepsilon_2^2 \lesssim w_d k_r$, for which this term is appreciable, have the probability $\sim\sqrt{w_d k_r}/\omega_{\mathrm{hf}} \ll 1$. Therefore, in this limit we neglect the second term of Eq. (29). For typical pairs under a weak resonant microwave one has $|x|, |y| \gg 1$, so the approximate relation,

$$\sin^2(2\phi_{\mathrm{eh}}) \approx \frac{4y^2}{(x^2-y^2)^2 + 4y^2}, \tag{36}$$

can be used with the first term of Eq. (29), leading to

$$\mathcal{L}(\omega_1) = \mathcal{L}_0\int dx dy \mathcal{P}(x)\mathcal{P}(y)\frac{y^2}{a^2(x^2-y^2)^2 + y^2}, \tag{37}$$

where

$$\mathcal{L}_0 = \frac{k_d k_r^2}{2w_d(2w_d + k_r)(4w_d + k_r)}, \quad a = \frac{\sqrt{2w_d(2w_d + k_r)}}{4w_d + k_r}. \tag{38}$$

For $a\beta_0 > 1$ ($\omega_1 < a\omega_{\mathrm{hf}}$) the integral (37) further simplifies, as in this case it is dominated by the narrow region, $||x| - |y|| \lesssim 1/a < \beta_0$. Due to the latter relation, the distribution of $|x| - |y|$

can be replaced by the constant, $1/\sqrt{2\pi}\beta_0$, and the resulting integral can be calculated. This gives

$$\frac{\mathcal{L}(\omega_1)}{\mathcal{L}_0} = \frac{\sqrt{\pi/2}}{a\beta_0} = \sqrt{\frac{\pi}{2a^2}}\frac{\omega_1}{\omega_{\rm hf}}. \tag{39}$$

The linear dependence equation Eq. (39) of PLDMR amplitude on ω_1 corresponds to $\propto\sqrt{P_{\rm mw}}$ dependence on the microwave power, $P_{\rm mw}$. This result agrees well with that of Ref. [13] and differs from the earlier predictions of $\propto P_{\rm mw}$ dependence [7,23].

3. *Strong resonant drive, $\omega_1 \gg \omega_{hf}$*

In the case of strong drive the second term of Eq. (29) is also important. In this case one typically has $|x|,|y| \ll 1$, and therefore the approximations

$$\sin^2(2\phi_{\rm eh}) \approx 4y^2, \quad \varepsilon_2 \approx \omega_1 xy, \tag{40}$$

can be used in the first and second terms of Eq. (29), respectively. Also, exploiting $2\omega_1 x \gg \sqrt{w_d k_r}$ ($\omega_{\rm hf} \gg \sqrt{w_d k_r}$), in the second term we replace $\cos^2(\phi_{\rm eh})$ by 1, neglecting a term $\sim y^2$. In terms of the constants,

$$b = \frac{\sqrt{2w_d(2w_d+k_r)}}{k_r}, \quad c = \frac{\sqrt{w_d(w_d+k_r)}}{\omega_{\rm hf}},$$
$$\mathcal{B} = \frac{(4w_d+k_r)^2}{k_r^2}, \quad \mathcal{C} = \frac{4w_d+k_r}{2(w_d+k_r)}, \tag{41}$$

and the universal functions

$$f_1(z) = z^2\int_{-\infty}^{\infty}\frac{d\rho}{\sqrt{\pi}}\frac{e^{-\rho^2}}{\rho^2+z^2} = \sqrt{\pi}\,z\exp(z^2)\mathrm{erfc}(z), \tag{42}$$

$$f_2(z) = z\int_0^{\infty} d\rho\frac{e^{-\rho}}{\sqrt{\rho^2+z^2}} = \frac{\pi}{2}z[H_0(z)-Y_0(z)], \tag{43}$$

where $\mathrm{erfc}(z)$ is the complementary error function, and $H_0(z)$, $Y_0(z)$ are the zero-order Struve and Bessel functions, respectively, our result reads

$$\frac{\mathcal{L}(\omega_1)}{\mathcal{L}_0} = \mathcal{B}[1-f_1(b\,\omega_1/\omega_{\rm hf})] - \mathcal{C}\,f_2(c\,\omega_1/\omega_{\rm hf}). \tag{44}$$

Considering the simple properties of $f_1(z)$ and $f_2(z)$, plotted in the Fig. 3 inset, this equation explains the decrease of $\mathcal{L}(\omega_1)$, Fig. 2, in simple terms. First we note that $b \lesssim 1$, $c \ll 1$, and $\mathcal{B} \approx \mathcal{C} \approx 1$. Thus, the domain $\omega_1 \gtrsim \omega_{\rm hf}$, next to the peak of $\mathcal{L}$, is dominated by the first term of Eq. (44). The last Dicke term of Eq. (44) becomes relevant for $\omega_1 \gg \omega_{\rm hf}$, where the first term vanishes. Finally, $\mathcal{C}$ gives the saturation value of $\mathcal{L}(\omega_1)/\mathcal{L}_0$.

The peak of $\mathcal{L}(\omega_1)$ occurs between the curves given by Eqs. (39) and (44). For $w_d \ll k_r$, entailing small $a \ll 1$, this domain is very narrow and the position of the peak, $\omega_1^{\max}$, is very close to the intersection of the two curves. From this argument one finds $\omega_1^{\max} \simeq \omega_{\rm hf} a\sqrt{2/\pi}$. The frequency ω_1^0 at which $\mathcal{L}$ becomes 0 can be estimated from the condition that f_1 in Eq. (44) is nearly 1. A good estimate for $f_1(z) \simeq 1$ is $z \simeq 5$, corresponding to $\omega_1^0 \simeq 5\omega_{\rm hf}/b$. Thus the characteristic values, $\omega_1^{\max}$ and ω_1^0, are expressed via $\omega_{\rm hf}$ and the kinetic parameters w_d and k_r. This is illustrated in Fig. 3, where we plot $\mathcal{L}(\omega_1)$ found by numerically solving Eq. (14), together with the asymptotes, Eqs. (39) and (44). In Fig. 3 we used the parameters inferred for a semiconducting fluorescent polymer [17], implying $w_d \ll k_r$.

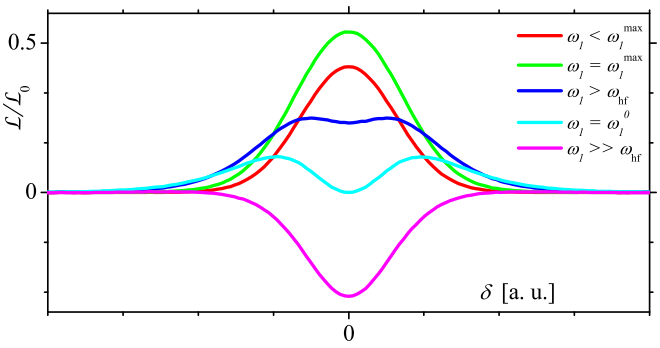

FIG. 4. Sketch of line shapes for different microwave amplitudes. Upon increasing the drive amplitude, the line (red) broadens and grows (green), and subsequently evolves to fully negative (magenta). Emergence of minimum (blue) manifests the onset of the spin-Dicke effect. Note that the plots are intended to assist the explanation and do not reflect any actual dependence.

E. Line-shape analysis

As illustrated in Fig. 4, the resonance lines can be divided into four groups by their shapes. At weak drive, corresponding to the region of initial linear growth in Fig. 2, the line shapes are double Gaussian. In the region near the maximum in Fig. 4, $\omega_1 \lesssim \omega_{\rm hf}$, the lines deviate from double Gaussian and become broader. The next, third group, including the lines with a minimum at resonance and two mirroring maxima at the sides, is found for $\omega_1 \gtrsim \omega_{\rm hf}$, and the fourth type of lines, showing completely negative resonance, appear at the strongest drives, $\omega_1 \gg \omega_{\rm hf}$. As discussed shortly, the two latter line shapes are clear fingerprints of the spin-Dicke effect.

The analytical forms of line shapes can be found from Eqs. (29) and (32), where the local Larmor frequencies are distributed by Eq. (5), with the nonzero detuning δ. At weak drive and for the general case of unequal electron and hole hyperfine coupling strengths, Eq. (37) is valid with a modification of the product, $\mathcal{P}(x)\mathcal{P}(y)$. The result of the asymptotic evaluation of the corresponding integral,

$$\frac{\mathcal{L}(\delta,\omega_1)}{\mathcal{L}_0} = \frac{\pi\omega_1}{2a}\left(\frac{e^{-\frac{\delta^2}{2\omega_{{\rm hf},e}^2}}}{\sqrt{2\pi}\,\omega_{{\rm hf},e}} + \frac{e^{-\frac{\delta^2}{2\omega_{{\rm hf},h}^2}}}{\sqrt{2\pi}\,\omega_{{\rm hf},h}}\right), \tag{45}$$

is the generalization of Eq. (39) for $\omega_{{\rm hf},e} \neq \omega_{{\rm hf},h}$. The red curve in Fig. 4 represents such a double Gaussian. Experimentally, this is the most easily accessible domain of drive. For stronger microwave strength, while the line shapes are still accurately described by Eqs. (29) and (32), only a qualitative analysis will follow.

The green curve in Fig. 4 is the line with the largest amplitude, occurring at $\omega_1 = \omega_1^{\max} < \omega_{\rm hf}$. It is broader than the double Gaussian Eq. (45). Both the red and green curves in Fig. 4 are well described by the first term of Eq. (29), meaning

that the Dicke subradiant state is not efficient at this microwave strength.

With the further increase of microwave strength over $\omega_{\rm hf}$, the line amplitudes decrease and central dips appear, as seen for the blue and cyan lines in Fig. 4. This signifies the onset of the subradiant mode, whose contribution is negative. The contribution of this mode overruns the regular term, which in turn becomes progressively smaller, at yet stronger microwave fields. In Fig. 4, the cyan line shows the situation where the signal is zero exactly at the resonance, and the magenta line depicts a fully negative resonance line. The latter represents the form at which the lines saturate at the strongest drives.

F. Finite spin-lattice relaxation

From Eqs. (12) and (15) it is easy to see that the operator U depends on the spin relaxation and the nonradiative decay only through the combination, $w_d = k_d + 1/T_{\rm sl}$. At slow spin relaxation the approximation Eq. (31) is valid, and therefore, up to an inessential overall factor, $\mathcal{L}$ also depends on w_d rather than on k_d or $T_{\rm sl}$. Thus, in the limit $1/T_{\rm sl} \ll k_d$, we encounter the conventional property of the additive inverse lifetimes.

To scrutinize the regime of intermediate spin relaxation, $1/T_{\rm sl} \gtrsim k_d$, we perform numerical simulations based on the exact formula Eq. (17). The results of our numerical analysis show that besides the additive feature of inverse lifetimes, the main effect of the spin relaxation is the overall reduction of the amplitude of $\mathcal{L}$. However, the latter effect is inessential because of the overall normalization uncertainty in real experimental conditions.

Figure 5 compares the finite spin relaxation results from the hyperfine averaged exact equation (17) with the outcome of the approximation Eq. (31). The parameters in Fig. 5 are borrowed from Ref. [17], where $1/T_{\rm sl} \simeq 5k_d$ is inferred experimentally. The solid lines in Fig. 5 are normalized to ensure the maximal value of 1 for the function, $\mathcal{L}(\delta,\omega_1)$, which occurs at $\omega_1 = \omega_1^{\rm max}$ and $\delta = 0$, both for the exact and the approximate solutions.

The plots in Figs. 5(a) and 5(b) clearly indicate very close results from the exact Eq. (17) and the approximation Eq. (31), thus confirming the additive character of spin relaxation and nonradiative decay rates for $\omega_1 \lesssim \omega_1^{\rm max}$ and moderate spin relaxation, $1/T_{\rm sl} \gtrsim k_d$. Deviations between the exact and approximate lines are noticeable in the domain of strong drive $\omega_1 > \omega_1^{\rm max}$, Fig. 5(c). Apparently, this could mean that the effect of spin relaxation can be resolved from that of the nonradiative recombination in the limit of strong drive. However, the approximate lines can be made very close to the exact ones upon applying different normalization factors for different ω_1 values, see Fig. 5(c). Therefore, in order to resolve the spin-relaxation effects, multiple resonance lines at different strong drive fields are necessary.

III. THE TRIPLET EXCITON-POLARON QUENCHING MODEL

Various schemes employing the triplet polaron quenching (TPQ) mechanism have been invoked in the literature to date [6,28–30]. Although different in many aspects, all these schemes stem from the spin-dependent reaction between a

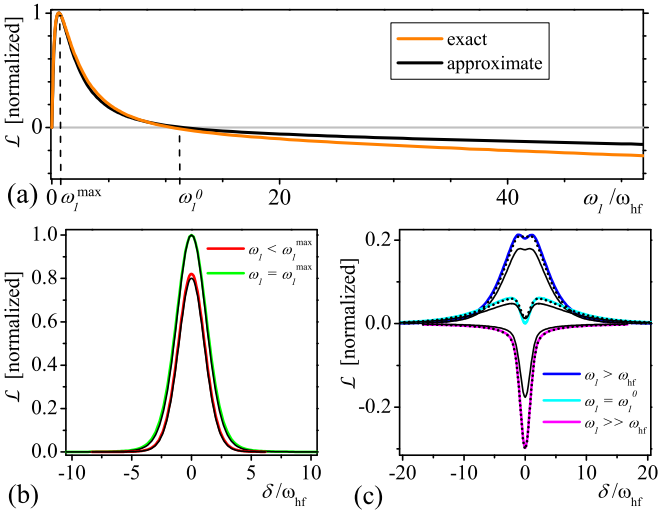

FIG. 5. Illustration of the role of spin-lattice relaxation in PPR model. Simulation results are shown for $T_{\rm sl} = 40\,\mu$s, $k_d = 5$ kHz, and $k_r = 230$ kHz (Ref. [17]). (a) The signal at resonant driving is plotted from the exact Eq. (17) with orange and from the approximate Eq. (31) with black. The plots are normalized to reach the maximum value of 1. (b, c) Line shapes for different microwave strengths are plotted in colors from Eq. (17), together with the corresponding plots from the approximate Eq. (31) (black lines). The normalization is the same as in (a). In the domain $\omega_1 \lesssim \omega_1^{\rm max}$, shown in (b), the approximate lines are very accurate, reflecting the additive character of spin relaxation and nonradiative decay. For $\omega_1 > \omega_1^{\rm max}$, illustrated in (c), the approximate curves deviate form the exact ones substantially. Still, approximate lines can be made very close to the exact ones with individual normalization for each ω_1 (black dots).

triplet exciton, TE, and a polaron, P:

$$\mathrm{TE} + \mathrm{P} \leftrightarrow \mathrm{P}^* + \mathrm{S}_0, \tag{46}$$

where S_0 stands for a singlet ground state and $*$ denotes a possibly excited state. While the right-hand side of Eq. (46) is spin doublet, the triplet exciton-polaron complex (TEP) in the left-hand side can form two different spin multiplets, a quartet and a doublet. Hence the spin dependence of the reaction (46), which can occur only from the doublet state of the initial complex. Furthermore, under magnetic resonance conditions, the TEP spin multiplicity, and therefore the reaction yield of Eq. (46), can be altered by a microwave drive.

The reaction (46) does not involve singlet excitons (SE), and the SE density, $n_{\rm S}$, becomes sensitive to the reaction yield because of a quenching of SEs by TEs and polarons. Ultimately, this quenching facilitates the optical detection of the microwave-induced reaction yield of Eq. (46). For simplicity, we will consider the quenching by TEs only, described by the rate equation

$$\partial_t n_{\rm S} = G_S - R_S n_{\rm S} - R_{ST} n_{\rm S} n_{\rm T}, \tag{47}$$

where the SE generation and decay rates, G_S and R_S, respectively, are the same as in Eq. (6), whereas R_{ST} is the SE-TE quenching rate. For the TE density $n_{\rm T}$ one has

$$\partial_t n_{\rm T} = G_T - R_T n_{\rm T} - R_{ST} n_{\rm T} n_{\rm S} - \beta(\delta,\omega_1) n_{\rm T}, \tag{48}$$

where G_T and R_T are, respectively, the TE generation and decay rates, and $\beta(\delta,\omega_1)$ is the rate of the TE population decline due to the reaction (46), which depends also on the polaron density n_P.

Under typical conditions, the nonlinear terms in Eqs. (47) and (48) are small perturbations, and the steady-state densities are quite accurately given by the first two terms in the rate equation right-hand sides:

$$\tilde{n}_S \approx G_S/R_S, \quad \tilde{n}_T \approx G_T/R_T. \tag{49}$$

Note that the description Eqs. (47)–(49) is valid for not very strong photoexcitation power P_L, ensuring a linear regime with $\tilde{n}_S \propto P_L$ ($G_S \propto P_L$).

In order to describe the magnetic-field effects, higher-order corrections to Eq. (49) must be considered. From Eqs. (47) and (48) we find

$$\tilde{n}_S = \sqrt{\left(\frac{R_T+\beta}{2R_{ST}} + \frac{G_T-G_S}{2R_S}\right)^2 + \frac{G_S(R_T+\beta)}{R_S R_{ST}}} - \left(\frac{R_T+\beta}{2R_{ST}} + \frac{G_T-G_S}{2R_S}\right). \tag{50}$$

The microwave-induced change of population, $\Delta\tilde{n}_S = \tilde{n}_S(\omega_1) - \tilde{n}_S(0)$, is found from Eq. (50) to be

$$\Delta\tilde{n}_S = \frac{\tilde{n}_S\tilde{n}_T R_{ST}}{R_S R_T}[\beta(\delta,\omega_1) - \beta(0)], \tag{51}$$

where we have used the leading-order results, Eq. (49), and the relation $G_S \gg G_T$.

We derive $\beta(\delta,\omega_1)$ in Appendix C from the stochastic Liouville approach by assuming that the steady-state TEP generation rate is given by the product $\lambda\tilde{n}_P\tilde{n}_T$, where λ is a constant determined by the TEP formation cross section. We get

$$\beta(\delta,\omega_1) = \lambda\tilde{n}_P\Gamma(\delta,\omega_1), \tag{52}$$

where $\Gamma(\delta,\omega_1)$ is governed by the TEP spin dynamics and recombination. Thus the (normalized) optically detected signal, $\Delta\mathcal{I}/\mathcal{I} = \Delta\tilde{n}_S/\tilde{n}_S$, is given by

$$\frac{\Delta\mathcal{I}(\delta,\omega_1)}{\mathcal{I}} = \tilde{n}_P\tilde{n}_T\frac{\lambda R_{ST}}{R_S R_T}[\Gamma(\delta,\omega_1) - \Gamma(0)]. \tag{53}$$

For the following discussion we present the zero-detuning result for $\Gamma(\omega_1) \equiv \Gamma(0,\omega_1)$, established in the limit of weak dissociation and recombination, and negligible coupling between the polaron and TE spins (see Appendix C). Figure 6 depicts the processes underlying the TPQ model. It includes the TEP generation rate g, the dissociation rate q_d, and the rate of the reaction Eq. (46) from the doublet manifold q_r. Not shown in Fig. 6 are the TEP spin-lattice relaxation time T_{sl} and the polaron hyperfine coupling magnitude ω_{hf}. In the limit of long spin coherence times, $T_{sl} > 1/q_d$, and slow dissociation and recombination, q_d, $q_r \ll \omega_{hf}$, we find $\Gamma(\omega_1) - \Gamma(0) = \Gamma_0 f_1(\omega_1/\omega_s)$, and therefore

$$\frac{\Delta\mathcal{I}(\omega_1)}{\mathcal{I}} = \tilde{n}_P\tilde{n}_T\frac{\lambda R_{ST}\Gamma_0}{R_S R_T}f_1(\omega_1/\omega_s), \tag{54}$$

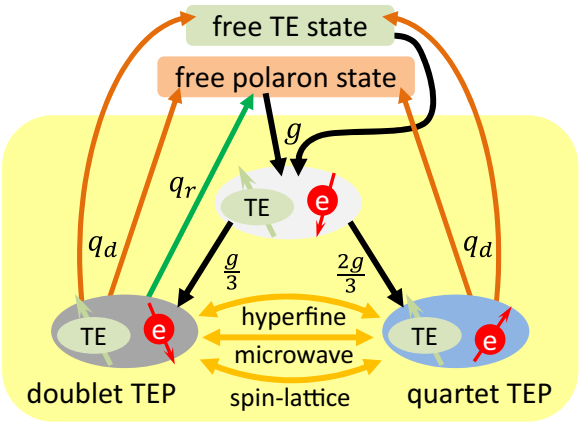

FIG. 6. Schematics of the processes involved in the TPQ model. The specifics of TPQ is that the microwave drive, together with the hyperfine coupling and spin-lattice relaxation, couples the TEP spin levels. The color code coincides with that in Fig. 1. The arrangement of the states is of no importance.

where

$$\Gamma_0 = \frac{2\,q_d\,q_r^2}{3v_d(3v_d+q_r)(3v_d+2q_r)},$$
$$\omega_s = \omega_{hf}\frac{\sqrt{6v_d(3v_d+2q_r)}}{3v_d+q_r}, \quad v_d = q_d + 1/T_{sl} \tag{55}$$

are constants. The function $f_1(z)$ appeared earlier in PPR model, see Eq. (42). It is plotted in Fig. 3 inset. It grows from zero linearly and saturates to unity at $z > 1$. This translates into the initially linear growth of $\Delta\mathcal{I}/\mathcal{I}$ and saturation to $\tilde{n}_P\tilde{n}_T\Gamma_0(\lambda R_{ST}/R_S R_T)$ at $\omega_1 > \omega_s$.

Note that Eq. (54) represents the contribution from only one species of polarons. To account for the other, charge-conjugated species, a term similar to that in the right-hand side of Eq. (54) must be included, with the corresponding values of λ, Γ_0, R_{ST}, R_S, R_T, and ω_s.

IV. DISCUSSION AND SUMMARY

The present study of the magnetic resonance-induced variation of singlet exciton recombination is based on the description of spin dynamics and recombination by means of stochastic Liouville equations. For the PPR model, we have demonstrated a solution method yielding the answer in terms of the eigenvalues of 4×4 complex Hamiltonian instead of the solution of effectively 10×10 complex linear system of stochastic Liouville equations. Analytical results supported by the direct numerical solution of stochastic Liouville equations are found in the limit of weak singlet recombination. The microwave-induced spin-Dicke effect, stemming from the backaction of recombination on the quantum dynamics of spin pairs, is identified and described quantitatively.

We have considered a spin-lattice relaxation, uniform with respect to the spin multiplicity. If the relaxation time is not too short, the main effect of this relaxation is additive to that of the dissociation and nonradiative recombination of the polaron pairs. We have shown that it can influence the resonance lines only at strong drive, whereas at weak drive it leads to the

overall scaling of resonance amplitudes. Note in passing that our approach naturally takes into account the dominant T_2 processes originating from the random hyperfine interaction.

Our analysis excludes the exchange and dipolar interactions between the spin pairs, although these interactions can be readily included in the presented perturbative scheme. This is done for the sake of simplicity, since our direct numerical simulations show that the effect of these interactions is minor, given that they do not exceed the average hyperfine coupling strength [18].

The TPQ model is treated along the same lines. However, calculations in this case are greatly simplified due to the presence of relatively strong zero-field splitting of triplets, making these states off resonance.

Concurring results are found from the PPR and TPQ models at weak drive. Namely, if the TPQ reaction Eq. (46) is equally probable for the electron and hole polarons, the line shapes from the two models are the same for $\omega_1 \ll \omega_{\rm hf}$ and are given by the sum of two Gaussians, Eq. (45).

More importantly, we uncover two substantial differences in the predictions of the PPR and the TPQ models. First and foremost, the dissimilar dependence of the microwave-induced signal on the steady-state densities,

$$\Delta\mathcal{I} \propto \tilde{n}_{\rm P}^2 \quad \text{(PPR)}, \quad \Delta\mathcal{I} \propto \tilde{n}_{\rm S}\tilde{n}_{\rm P}\tilde{n}_{\rm T} \quad \text{(TPQ)}, \tag{56}$$

cf. Eqs. (19) and (54), respectively, leads to the remarkably different results for the dependence of $\Delta\mathcal{I}/\mathcal{I}$ on the photoexcitation power, P_L. Far from saturation at high P_L it is reasonable to expect that $\tilde{n}_{\rm S} \propto P_L$, $\tilde{n}_{\rm P} \propto P_L$, and $\tilde{n}_{\rm T} \propto P_L$ crossing over to $\tilde{n}_{\rm T} \propto P_L^2$. (The position of crossover depends on the efficiency of the intersystem crossing from SE to TE and the TE generation from nongeminate polaron pairs [31].) For the TPQ model, this results in $\Delta\mathcal{I}/\mathcal{I} \propto P_L^2$ to P_L^3, in contrast to the PPR prediction, $\Delta\mathcal{I}/\mathcal{I} \propto P_L$.

The second important difference between the predictions of the two models comes from the fact that at the polaron spin-1/2 resonance, TEs are mainly off resonance because of a relatively strong zero-field splitting. As a result, the line shapes and the saturation behavior from the two models are different at strong drive. Specifically, the TPQ leads to the resonance lines featuring a single maximum and relatively fast saturation of $\Delta\mathcal{I}/\mathcal{I}$ to positive values at $\omega_1 \approx \omega_{\rm hf}$, much like in the ordinary electron spin resonance. In contrast, the PPR model predicts resonance lines with two maxima around the central dip at $\omega_1 \gtrsim \omega_{\rm hf}$, evolving into the completely negative resonance at $\omega_1 \gg \omega_{\rm hf}$, where $\Delta\mathcal{I}/\mathcal{I}$ saturates to negative values (see Figs. 2 and 4). These differences are of relevance for resolving the contributions of the two mechanisms experimentally via continuous-wave PLDMR measurements.

Finally, we note that this study did not address the predictions for the observables which are measured using the double-modulation (DM) PLDMR technique [6,8]. In this technique the laser excitation power is modulated at certain frequency f_L, and a lock-in amplifier filters out the delayed photoluminescence that is slower than f_L. Therefore, by the design, the DM-PLDMR measures only the prompt component of the photoluminescence. The results obtained using the DM-PLDMR [6,8] are independent of f_L up to 100 kHz. In this regard, we would like to note that our Eq. (56) offers a certain prediction for DM-PLDMR. Namely, the proportionality of $\Delta\mathcal{I}$ to $\tilde{n}_{\rm S}$ renders the interpretation of the DM-PLDMR results [4,6,8] in favor of the TPQ model. Further theoretical studies aimed at more quantitative predictions for DM-PLDMR are underway.

ACKNOWLEDGMENTS

We thank H. Malissa for helpful discussions. Work at the Ames Laboratory was supported by the U.S. Department of Energy, Office of Science, Basic Energy Sciences, Division of Materials Sciences and Engineering. The Ames Laboratory is operated for the U.S. Department of Energy by Iowa State University under Contract No. DE-AC02-07CH11358. M.R. acknowledges the support of the U.S. Department of Energy, Office of Basic Energy Sciences, Grant No. DE-FG02-06ER46313.

APPENDIX A

In this Appendix we discuss the relation between the stochastic Liouville equation (8) and an underlying Lindblad equation, as well as elaborate on the rotating-frame transformation of Eq. (8).

1. Lindblad formulation of the PPR model

The most general Markovian quantum dynamics of an open system can be described by a Lindblad equation [32]. In our subsequent consideration of this formalism we will closely follow Ref. [33]. In addition to the four spin-pair states T_1, T_0, T_{-1}, S, the full Lindblad description of the PPR would require the introduction of the radiative singlet exciton and free polaron states, $X_{\rm rs}$ and $X_{\rm fp}$, respectively. The Lindblad equation for the corresponding (6×6) full density matrix of the system ϱ is given by [33]

$$\frac{d\varrho}{dt} = i[\varrho, H] + \sum_{j=1}^{N_c}\left(c_j\varrho c_j^\dagger - \frac{1}{2}c_j^\dagger c_j\varrho - \frac{1}{2}\varrho c_j^\dagger c_j\right), \tag{A1}$$

with N_c system operators, c_j. Here, the spin relaxation processes involve 16 system operators, $c_{\alpha\beta} = (4T_{\rm sl})^{-1/2}|\alpha\rangle\langle\beta|$, where $\alpha, \beta = T_1, T_0, T_{-1}, S$. Furthermore, according to the definition of PPR model, Fig. 1, the recombination, dissociation, and generation processes involve nine system operators: one associated with the recombination, $c_{r,S} = \sqrt{k_r}|X_{\rm rs}\rangle\langle S|$, four with the dissociation, $c_{d,\alpha} = \sqrt{k_d}|X_{\rm fp}\rangle\langle\alpha|$, and four more associated with the polaron pair generation, $c_{g,\alpha} = \sqrt{g_0}|\alpha\rangle\langle X_{\rm fp}|$.

Now it is straightforward to check that the action of the first 16 system operators leads to the spin-lattice relaxation term Eq. (11) of the reduced PP spin density matrix $\rho_{\alpha\beta} = \langle\alpha|\varrho|\beta\rangle$:

$$\langle\alpha|\sum_{j=\alpha'\beta'}\left(c_j\varrho c_j^\dagger - \frac{1}{2}c_j^\dagger c_j\varrho - \frac{1}{2}\varrho c_j^\dagger c_j\right)|\beta\rangle = \mathcal{R}_{\rm sl}\{\rho\}_{\alpha\beta}. \tag{A2}$$

For the nine remaining system operators we have

$$\langle\alpha|\sum_k\left(c_k\varrho c_k^\dagger - \frac{1}{2}c_k^\dagger c_k\varrho - \frac{1}{2}\varrho c_k^\dagger c_k\right)|\beta\rangle = \mathcal{R}_{\rm dr}\{\rho\}_{\alpha\beta} + g_0\langle X_{\rm fp}|\varrho|X_{\rm fp}\rangle\delta_{\alpha\beta}, \tag{A3}$$

where the summation runs over $k = (r,S)$, (d,α), and (g,α). Thus, the stochastic Liouville equation Eq. (8) emerges from Eq. (A1) as the result of a physically transparent assumption that the free polaron population is time-independent, and the polaron pair generation rate, $g = 4g_0\langle X_{\rm fp}|\varrho|X_{\rm fp}\rangle$, is constant.

2. Rotating-frame transformation of Eq. (8)

The rotating-frame transformation applied while going from Eq. (8) to Eq. (9) implies the time-dependent unitary transformation with the operator, $U = \exp[i\omega t(S_e^z + S_h^z)]$. In particular, for the density matrix we have $\rho = U\rho_L U^\dagger$, where ρ is the rotating-frame density matrix used throughout the text and ρ_L is the laboratory-frame density matrix. For the dissipative terms in the laboratory frame we have

$$\mathcal{R}_{\rm dr}\{\rho_L\} = -k_d\rho_L - \frac{k_r}{2}\{\Pi_S,\rho_L\},$$
$$\mathcal{R}_{\rm sl}\{\rho_L\} = -\frac{1}{T_{\rm sl}}[\rho_L - {\rm tr}(\rho_L/4)\mathbb{1}],$$

where Π_S is the projection operator onto the singlet state and $\{\cdot,\cdot\}$ means the anticommutation. Applying the rotating-frame transformation to $\mathcal{R}_{\rm sl}\{\rho_L\}$ gives

$$U\mathcal{R}_{\rm sl}\{\rho_L\}U^\dagger = -\frac{1}{T_{\rm sl}}[\rho - {\rm tr}(\rho/4)\mathbb{1}], \tag{A4}$$

where we have used $\rho = U\rho_L U^\dagger$ and the invariance of the trace, ${\rm tr}(\rho_L) = {\rm tr}(\rho)$. In the case of $\mathcal{R}_{\rm dr}\{\rho_L\}$ we get

$$\begin{aligned} U\mathcal{R}_{\rm dr}\{\rho_L\}U^\dagger &= -k_d\rho - \frac{k_r}{2}\{U\Pi_S U^\dagger,\rho\} \\ &= -k_d\rho - \frac{k_r}{2}\{\Pi_S,\rho\}, \end{aligned} \tag{A5}$$

the last relation following from the invariance of projection operator, $U\Pi_S U^\dagger = \Pi_S$. The latter invariance means that the rotating-frame transformation does not alter the spin multiplicity. This, in turn, can be seen by writing $\Pi_S = 1/4 - \mathbf{S}_e\mathbf{S}_h$ and using the vanishing commutator, $[(S_e^z + S_h^z),\mathbf{S}_e\mathbf{S}_h] = 0$, leading to $[U,\Pi_S] = 0$.

Equations (A4) and (A5) establish the invariance of the dissipative terms with respect to the rotating-frame transformation.

APPENDIX B

In this Appendix we investigate the steady-state Liouville equation for the PPR model, Eq. (14). Because of the non-Hermitian character of the Hamiltonian $\mathcal{H}$, Eq. (12), the calculation of ${\rm tr}\,U$ is specific. We introduce the eigenvectors and eigenvalues, $\mathcal{H}|\psi_\alpha\rangle = \varepsilon_\alpha|\psi_\alpha\rangle$, $\alpha = 1,..,4$. As the non-Hermitian Hamiltonian $\mathcal{H}$ is symmetric, the conjugated equation $\langle\psi_\alpha|\mathcal{H} = \varepsilon_\alpha\langle\psi_\alpha|$ holds for $\langle\psi_\alpha| = |\psi_\alpha\rangle^{\intercal}$, where the superscript $^{\intercal}$ means the transpose without a complex conjugation. We normalize the eigenvectors with respect to this conjugation, so that $\langle\psi_\alpha||\psi_\alpha\rangle = 1$. It is also easy to check that the eigenvectors are orthogonal; $\langle\psi_\alpha||\psi_\beta\rangle \equiv \sum_{n=1}^4 \psi_\alpha(n)\psi_\beta(n) = 0$, if $\varepsilon_\alpha \neq \varepsilon_\beta$, whereas the degenerate case can be handled in the standard way by choosing orthogonal vectors in the degenerate subspace. Thus $\{|\psi_\alpha\rangle\}_{\alpha=1}^4$ can be made a complete orthonormal set. This ensures the partition of unity, $\sum_{\alpha=1}^4 |\psi_\alpha\rangle\langle\psi_\alpha| = \mathbb{1}$, yielding ${\rm tr}\,U = \sum_{\alpha=1}^4\langle\psi_\alpha|U|\psi_\alpha\rangle$. The complex conjugate vectors, $|\psi_\alpha^*\rangle \equiv |\psi_\alpha\rangle^*$, obeying $\mathcal{H}^*|\psi_\alpha^*\rangle = \varepsilon_\alpha^*|\psi_\alpha^*\rangle$, form another orthonormal set, in general different from $\{|\psi_\alpha\rangle\}_{\alpha=1}^4$. With these conventions, from Eq. (15) we write

$${\rm tr}\,U = \sum_{\alpha,\beta=1}^4 \frac{\langle\psi_\alpha||\psi_\beta^*\rangle\langle\psi_\beta^*||\psi_\alpha\rangle}{i(\varepsilon_\alpha - \varepsilon_\beta^*)}. \tag{B1}$$

Treating the recombination term of the Hamiltonian (12), $V = -i(k_r/2)\Pi_S$, as a perturbation, we get

$$\langle\psi_\alpha||\psi_\beta^*\rangle\langle\psi_\beta^*||\psi_\alpha\rangle = \delta_{\alpha\beta} + \mathcal{O}(k_r/\Omega_{e,h})^2 \tag{B2}$$

and

$$\varepsilon_\alpha = \epsilon_\alpha - i(w_d/2) + V_{\alpha\alpha} + \mathcal{O}\big(k_r^2/\Omega_{e,h}\big), \tag{B3}$$

where ϵ_α are the eigenvalues of the Hamiltonian H, Eq. (9). By observing that the $\sim k_r^2/\Omega_{e,h}$ correction in ε_α is real, from Eqs. (B1)–(B3) we infer that omitting the inexplicit terms in Eqs. (B2), (B3) induces only $\sim(k_r/\Omega_{e,h})^2{\rm tr}\,U$ error in ${\rm tr}\,U$. Therefore, rather accurate results can be found by completely neglecting the eigenvector corrections and keeping only the leading corrections to ε_α. This is as much as we get from Eq. (B1), because the degeneracy of H makes the simple perturbation calculation inefficient.

Still, the explicit form of the unperturbed eigenstates of $\mathcal{H}$, $|\varphi_\alpha\rangle$, which are the eigenvectors of H, is needed. In the absence of the exchange and dipolar interactions, the individual electron ($\mu = e$) and hole ($\mu = h$) polaron eigenstates are

$$\begin{aligned} |\Uparrow\rangle_\mu &= \cos\phi_\mu|\uparrow\rangle_\mu + \sin\phi_\mu|\downarrow\rangle_\mu, \\ |\Downarrow\rangle_\mu &= \sin\phi_\mu|\uparrow\rangle_\mu - \cos\phi_\mu|\downarrow\rangle_\mu, \end{aligned} \tag{B4}$$

where $|\uparrow\rangle_\mu, |\downarrow\rangle_\mu$ are the electron- and hole-polaron spin-up and -down states with the quantization axes along $\hat{\mathbf{z}}$, and $\tan 2\phi_\mu = \omega_1/\omega_\mu$ is introduced. Then we have

$$\begin{aligned} |\varphi_1\rangle &= |\Uparrow\rangle_e|\Uparrow\rangle_h, \quad |\varphi_2\rangle = |\Uparrow\rangle_e|\Downarrow\rangle_h, \\ |\varphi_3\rangle &= |\Downarrow\rangle_e|\Uparrow\rangle_h, \quad |\varphi_4\rangle = |\Downarrow\rangle_e|\Downarrow\rangle_h. \end{aligned} \tag{B5}$$

The matrix $V_{\alpha\beta} = \langle\varphi_\alpha|V|\varphi_\beta\rangle$, Eq. (23) in the main text, is found by calculating the scalar products of $|\varphi_\alpha\rangle$ with $|S\rangle$.

The degeneracy of H, controlling the strong drive regime, corresponds to $\phi_\mu \approx \pi/4$. Then Eqs. (2), (B4), and (B5) give

$$\begin{aligned} |\varphi_1\rangle &\approx \tfrac{1}{2}(|T_{+1}\rangle + |T_{-1}\rangle + \sqrt{2}\,|T_0\rangle), \\ |\varphi_2\rangle &\approx \tfrac{1}{2}(|T_{+1}\rangle + |T_{-1}\rangle - \sqrt{2}\,|S\rangle), \\ |\varphi_3\rangle &\approx \tfrac{1}{2}(|T_{+1}\rangle + |T_{-1}\rangle + \sqrt{2}\,|S\rangle), \\ |\varphi_4\rangle &\approx \tfrac{1}{2}(|T_{+1}\rangle + |T_{-1}\rangle - \sqrt{2}\,|T_0\rangle). \end{aligned} \tag{B6}$$

The vectors $|\varphi_1\rangle$ and $|\varphi_4\rangle$ are always the eigenstates of $\mathcal{H}$ to the leading order, whereas $|\varphi_2\rangle$ and $|\varphi_3\rangle$ are not such in the vicinity of the degeneracy of H. On the other hand, the eigenvectors of $\tilde{\mathcal{H}} = H - i(w_d/2)\mathbb{1} + \tilde{V}$, where $\tilde{V}$ is given by Eq. (28) in the main text, are always the leading order eigenstates of $\mathcal{H}$. In addition, $\mathcal{H}$ and $\tilde{\mathcal{H}}$ have the same eigenvalues within the first subleading order. Thus, by virtue of the arguments presented

after Eq. (B3), one can replace $\mathcal{H}$ by $\tilde{\mathcal{H}}$ in Eq. (15) of the main text and calculate $\mathrm{tr}\,U$ with a satisfactory precision, regardless of the degeneracy. The calculation of $\mathrm{tr}\,U$ is facilitated by fact that $\tilde{\mathcal{H}}$ is diagonal in the (φ_1,φ_4) subspace, whereas the contribution of the (φ_2,φ_3) subspace can be found by using the formula

$$e^{i(x\sigma_x+y\sigma_z)} = \cos r + i(x\sigma_x + y\sigma_z)\sin r/r, \tag{B7}$$

where $\sigma_{x,z}$ are the Pauli matrices, and $r=\sqrt{x^2+y^2}$. This gives

$$\mathrm{tr}\,U = \frac{4}{k_r\sin^2(\phi_{\rm eh})+2w_d} + \frac{4}{k_r\cos^2(\phi_{\rm eh})+2w_d} + \frac{k_r^2\cos^4(\phi_{\rm eh})}{[k_r\cos^2(\phi_{\rm eh})+2w_d]\big[4\varepsilon_2^2+w_d(k_r\cos^2(\phi_{\rm eh})+w_d)\big]}, \tag{B8}$$

where the first term comes from the (φ_1,φ_4), and the last two terms from the (φ_2,φ_3) manifolds. Combining the first two terms gives Eq. (29) of the main text.

APPENDIX C

In this Appendix we derive the rate $\beta(\delta,\omega_1)$, introduced in Eq. (48) of the main text, in the limit of negligible exchange and dipolar coupling between the TE and polaron spins, and weak dissociation and recombination.

The basis spin states of a TEP complex can be given through the direct product of a triplet and doublet states, as well as through the direct sum of a quartet and doublet multiplets, via the Clebsch-Gordan coefficients. In terms of the components, $T_0, T_{\pm1}$, representing triplet excitons with spin projection 0 and ±1, respectively, and $\uparrow,\downarrow$ for polaron spin $\pm1/2$, we have

$$\begin{aligned}
|T_{+1}\uparrow\rangle &= Q_{3/2},\\
|T_{+1}\downarrow\rangle &= \sqrt{1/3}\,Q_{1/2}+\sqrt{2/3}\,D_{1/2},\\
|T_0\uparrow\rangle &= \sqrt{2/3}\,Q_{1/2}-\sqrt{1/3}\,D_{1/2},\\
|T_0\downarrow\rangle &= \sqrt{2/3}\,Q_{-1/2}+\sqrt{1/3}\,D_{-1/2},\\
|T_{-1}\uparrow\rangle &= \sqrt{1/3}\,Q_{-1/2}-\sqrt{2/3}\,D_{-1/2},\\
|T_{-1}\downarrow\rangle &= Q_{-3/2},
\end{aligned} \tag{C1}$$

where Q_k and D_k are the quartet and doublet states with the spin projection k.

The 6×6 spin density matrix of an ensemble of TEP complexes ϱ can be treated by a stochastic Liouville equation. Formally, the Liouville equation for ϱ is found by rewriting Eq. (8) with the following modifications:

(i) The rotating-frame spin Hamiltonian H is given by

$$H = \omega_{\rm P}S_z + H_{0,T} + \omega_1(I_x+S_x), \tag{C2}$$

where $\omega_{\rm P}$ is the polaron Larmor frequency, $\mathbf{S}=1/2$ and $\mathbf{I}=1$ are the polaron and TE spin operators, and

$$H_{0,T} = \omega_T I_z + \mathcal{D}\big[I_z^2 - I(I+1)/3\big] \tag{C3}$$

is the free TE spin Hamiltonian with the TE Larmor frequency, $\omega_T=\gamma_T\hbar(B_0+b_T^z)-\omega$, and the axial zero-field splitting parameter $\mathcal{D}$. (The transverse zero-field splitting is neglected in the secular approximation.) We take equal gyromagnetic ratios [4] of TEs and polarons; $\gamma_T=\gamma_{e,h}$.

(ii) The generation rate, second term in Eq. (8), is replaced by $(g/6)\mathbb{1}$, implying equal probability of the TEP generation in six different spin states. Similarly, the factors of $1/4$ in the last terms of Eqs. (11) and (13) are replaced by $1/6$.

(iii) The dissociation-recombination rates are denoted, respectively, by q_d and q_r, so that Eq. (10) goes into

$$\mathcal{R}_{\rm dr}\{\varrho\}_{\alpha\beta} = -q_d\varrho_{\alpha\beta} - \frac{q_r}{2}\sum_{\sigma=\pm\frac12}(\delta_{\alpha D_\sigma}+\delta_{D_\sigma\beta})\varrho_{\alpha\beta}, \tag{C4}$$

implying a recombination from the doublet TEP states.

(iv) The second term in Eq. (12) is written as $-i(v_d/2)\mathbb{1}$, where $v_d=q_d+1/T_{\rm sl}$, and, more importantly, the operator Π_S is replaced by the projection operator onto the doublet,

$$\Pi_D = |D_{1/2}\rangle\langle D_{1/2}| + |D_{-1/2}\rangle\langle D_{-1/2}|. \tag{C5}$$

We further assume that the TEP generation rate is proportional to $n_{\rm T}$ and $n_{\rm P}$, $g=\lambda n_{\rm T}n_{\rm P}$, and that after dissociation of a TEP complex, the constituent TE returns into the state described by $n_{\rm T}$ (see Fig. 6). The latter assumption allows us to write the TEP counterpart of Eq. (16), $\beta\tilde{n}_{\rm T} = g - q_d\,\mathrm{tr}\tilde{\varrho}$, where g gives the rate of the decrease of $n_{\rm T}$ due to the generation of TEP, and the last term reflects the increase of $n_{\rm T}$ because of dissociation. By virtue of the full analogy with PPR model, see Eq. (17), we write

$$\beta(\delta,\omega_1) = \lambda\tilde{n}_{\rm P}\Gamma(\delta,\omega_1), \quad \Gamma = \left\langle \frac{1-\frac{v_d}{6}\mathrm{tr}\bar{U}}{1-\frac{1}{6T_{\rm sl}}\mathrm{tr}\bar{U}} \right\rangle_{\rm hf}, \tag{C6}$$

where $\bar{U}$ is given by the TPQ counterpart of Eq. (15).

Despite that the TE and polaron gyromagnetic ratios are taken to be the same [4], the majority of TE spins are off resonance because of the relatively strong zero-field splitting. In Eq. (C2) we have $\mathcal{D}=\mathcal{D}_0(3\cos^2\theta-1)/2$, where θ is the angle between the zero-field tensor principal z axis and $\hat{\mathbf{z}}$, and $\mathcal{D}_0\gtrsim 500$ G is measured for several polymer PPV derivatives [4]. The portion of near-resonance TEs is $\sim\omega_1/\mathcal{D}_0$, and most of these TEs are still off resonance because of the nonzero TE hyperfine coupling. Therefore, we calculate $\mathrm{tr}\bar{U}$ to the leading order in $\omega_1/\mathcal{D}_0$ and $\omega_{\rm hf}/\mathcal{D}_0$, corresponding to the perturbation

$$\bar{V} = -i(q_r/2)\Pi_D + \omega_1(I_x+S_x). \tag{C7}$$

The left-hand side states in Eq. (C1) are then the unperturbed eigenstates. Because of the $\sim\mathcal{D}_0$ energy splitting between $|T_{+1}\uparrow,\downarrow\rangle$ and $|T_0\uparrow,\downarrow\rangle$, and between $|T_{-1}\uparrow,\downarrow\rangle$ and $|T_0\uparrow,\downarrow\rangle$, the matrix elements of $\bar{V}$, relevant to the leading order, are

those between the same T_i states, explicitly given by

$$\bar{V} \simeq \begin{pmatrix} 0 & \frac{\omega_1}{2} & \cdot & \cdot & \cdot & \cdot \\ \frac{\omega_1}{2} & -\frac{iq_r}{3} & \cdot & \cdot & \cdot & \cdot \\ \cdot & \cdot & -\frac{iq_r}{6} & \frac{\omega_1}{2} & \cdot & \cdot \\ \cdot & \cdot & \frac{\omega_1}{2} & -\frac{iq_r}{6} & \cdot & \cdot \\ \cdot & \cdot & \cdot & \cdot & -\frac{iq_r}{3} & \frac{\omega_1}{2} \\ \cdot & \cdot & \cdot & \cdot & \frac{\omega_1}{2} & 0 \end{pmatrix}. \quad \text{(C8)}$$

The structure of the matrix (C7) indicates that the system reduces to three two-level subsystems, which are decoupled in the leading order. Further calculation of $\mathrm{tr}\bar{U}$ is done by using Eq. (B7) for each of the three subsystems, yielding

$$\mathrm{tr}\bar{U} = \frac{2}{v_{dr}} + \frac{2v_{dr}\left[v_{dr}^2 + \omega_{\mathrm{P}}^2 + \omega_1^2\right]}{\left[v_{dr}^2 + \omega_{\mathrm{P}}^2\right]\left[v_{dr}^2 - q_r^2/9\right] + v_{dr}^2\omega_1^2}, \quad \text{(C9)}$$

where $v_{dr} = v_d + q_r/3$. The hyperfine average in Eq. (C6) is over the Gaussian distribution of ω_{P}, given by Eq. (5). By expanding the denominator in Eq. (C6) over the small $\mathrm{tr}\bar{U}/T_{\mathrm{sl}}$ and using Eq. (C9) we get

$$\Gamma(\omega_1) - \Gamma(0) = \Gamma_0\left(\frac{\omega_1}{\omega_s}\right)^2 \int_{-\infty}^{\infty} \frac{dz}{\sqrt{\pi}} \frac{\exp(-z^2)}{z^2 + (\omega_1/\omega_s)^2}, \quad \text{(C10)}$$

found by neglecting $v_{dr}^2/2\omega_{\mathrm{hf}}^2 \ll 1$ in the denominator. This integral happens to coincide with Eq. (42) for $f_1(z)$, leading to the result, Eq. (54).

[1] B. C. Cavenett, Optically detected magnetic resonance (O.D.M.R.) investigations of recombination processes in semiconductors, Adv. Phys. **30**, 475 (1981).

[2] R. A. Street, Recombination in α-Si: H: Spin-dependent effects, Phys. Rev. B **26**, 3588 (1982).

[3] S. Depinna, B. C. Cavenett, I. G. Austin, T. M. Searle, M. J. Thompson, J. Allison, and P. G. L. Comberd, Characterization of radiative recombination in amorphous silicon by optically detected magnetic resonance: Part I, Philos. Mag. B **46**, 473 (1982).

[4] J. Shinar, Optically detected magnetic resonance studies of luminescence-quenching processes in π-conjugated materials and organic light-emitting devices, Laser Photon. Rev. **6**, 767 (2012).

[5] M. Wohlgenannt, K. Tandon, S. Mazumdar, S. Ramasesha, and Z. V. Vardeny, Formation cross-sections of singlet and triplet excitons in π-conjugated polymers, Nature (London) **409**, 494 (2001).

[6] M.-K. Lee, M. Segal, Z. G. Soos, J. Shinar, and M. A. Baldo, Yield of Singlet Excitons in Organic Light-Emitting Devices: A Double Modulation Photoluminescence-Detected Magnetic Resonance Study, Phys. Rev. Lett. **94**, 137403 (2005).

[7] C. G. Yang, E. Ehrenfreund, and Z. V. Vardeny, Polaron Spin-Lattice Relaxation Time in π-Conjugated Polymers from Optically Detected Magnetic Resonance, Phys. Rev. Lett. **99**, 157401 (2007).

[8] M. Segal, M. A. Baldo, M. K. Lee, J. Shinar, and Z. G. Soos, Frequency response and origin of the spin-1/2 photoluminescence-detected magnetic resonance in a π-conjugated polymer, Phys. Rev. B **71**, 245201 (2005).

[9] Y. Chen, M. Cai, E. Hellerich, R. Shinar, and J. Shinar, Origin of the positive spin-1/2 photoluminescence-detected magnetic resonance in π-conjugated materials and devices, Phys. Rev. B **92**, 115203 (2015).

[10] C. G. Yang, E. Ehrenfreund, F. Wang, T. Drori, and Z. V. Vardeny, Spin-dependent kinetics of polaron pairs in organic light-emitting diodes studied by electroluminescence detected magnetic resonance dynamics, Phys. Rev. B **78**, 205312 (2008).

[11] S.-Y. Lee, S.-Y. Paik, D. R. McCamey, J. Yu, P. L. Burn, J. M. Lupton, and C. Boehme, Tuning hyperfine fields in conjugated polymers for coherent organic spintronics, J. Am. Chem. Soc. **133**, 2019 (2011).

[12] R. C. Roundy and M. E. Raikh, Slow dynamics of spin pairs in a random hyperfine field: Role of inequivalence of electrons and holes in organic magnetoresistance, Phys. Rev. B **87**, 195206 (2013).

[13] R. C. Roundy and M. E. Raikh, Organic magnetoresistance under resonant ac drive, Phys. Rev. B **88**, 125206 (2013).

[14] V. S. L'vov, L. S. Mima, and O. V. Tretyak, Investigation of spin-dependent recombination in semiconductors, Sov. Phys. JETP **56**, 897 (1982).

[15] A. V. Barabanov, O. V. Tretiak, and V. A. L'vov, Complete theoretical analysis of the Kaplan-Solomon-Mott mechanism of spin-dependent recombination in semiconductors, Phys. Rev. B **54**, 2571 (1996).

[16] D. R. McCamey, K. J. van Schooten, W. J. Baker, S.-Y. Lee, S.-Y. Paik, J. M. Lupton, and C. Boehme, Hyperfine-Field-Mediated Spin Beating in Electrostatically Bound Charge Carrier Pairs, Phys. Rev. Lett. **104**, 017601 (2010).

[17] D. R. McCamey, H. A. Seipel, S.-Y. Paik, M. J. Walter, N. J. Borys, J. M. Lupton, and C. Boehme, Spin Rabi flopping in the photocurrent of a polymer light-emitting diode, Nat. Mater. **7**, 723 (2008).

[18] K. J. van Schooten, D. L. Baird, M. E. Limes, J. M. Lupton, and C. Boehme, Probing long-range carrier-pair spin–spin interactions in a conjugated polymer by detuning of electrically detected spin beating, Nat. Commun. **6**, 6688 (2015).

[19] D. P. Waters, G. Joshi, M. Kavand, M. E. Limes, H. Malissa, P. L. Burn, J. M. Lupton, and C. Boehme, The spin-Dicke effect in OLED magnetoresistance, Nat. Phys. **11**, 910 (2015).

[20] S. L. Bayliss, N. C. Greenham, R. H. Friend, H. Bouchiat, and A. D. Chepelianskii, Spin-dependent recombination probed through the dielectric polarizability, Nat. Commun. **6**, 8534 (2015).

[21] C. Boehme and K. Lips, Theory of time-domain measurement of spin-dependent recombination with pulsed electrically detected magnetic resonance, Phys. Rev. B **68**, 245105 (2003).

[22] R. Glenn, W. J. Baker, C. Boehme, and M. E. Raikh, Analytical description of spin-Rabi oscillation controlled electronic transitions rates between weakly coupled pairs of paramagnetic states with $S = 1/2$, Phys. Rev. B **87**, 155208 (2013).

[23] T. Eickelkamp, S. Roth, and M. Mehring, Electrically detected magnetic resonance in photoexcited fullerenes, Mol. Phys. **95**, 967 (1998).

[24] L. D. Landau and L. M. Lifshitz, *Quantum Mechanics, Non-Relativistic Theory* (Butterworth-Heinemann, Oxford, 1981), Vol. 3.

[25] R. H. Dicke, Coherence in spontaneous radiation processes, Phys. Rev. **93**, 99 (1954).

[26] N. J. Harmon and M. E. Flatté, Semiclassical theory of magnetoresistance in positionally disordered organic semiconductors, Phys. Rev. B **85**, 075204 (2012).

[27] C. P. Slichter, *Principles of Magnetic Resonance* (Harper & Row, New York, 1963).

[28] P. Desai, P. Shakya, T. Kreouzis, and W. P. Gillin, Magnetoresistance in organic light-emitting diode structures under illumination, Phys. Rev. B **76**, 235202 (2007).

[29] J. Y. Song, N. Stingelin, A. J. Drew, T. Kreouzis, and W. P. Gillin, Effect of excited states and applied magnetic fields on the measured hole mobility in an organic semiconductor, Phys. Rev. B **82**, 085205 (2010).

[30] A. J. Schellekens, W. Wagemans, S. P. Kersten, P. A. Bobbert, and B. Koopmans, Microscopic modeling of magnetic-field effects on charge transport in organic semiconductors, Phys. Rev. B **84**, 075204 (2011).

[31] E. J. W. List, C.-H. Kim, A. K. Naik, U. Scherf, G. Leising, W. Graupner, and J. Shinar, Interaction of singlet excitons with polarons in wide band-gap organic semiconductors: A quantitative study, Phys. Rev. B **64**, 155204 (2001).

[32] G. Lindblad, On the generators of quantum dynamical semigroups, Commun. Math. Phys. **48**, 119 (1976).

[33] P. Zoller and C. W. Gardiner, Quantum noise in quantum optics: The stochastic Schrödinger equation, arXiv:quant-ph/9702030.